

Design and Optimization of a New Structure PCB Coreless-type Linear Motor

Lingchen Li
Faculty of Mechanical Engineering and
Mechanics, Ningbo University;
Ningbo Institute of Materials Technology and
Engineering, Chinese Academy of Sciences
Ningbo, China
lilingchen@nimte.ac.cn

Jie Zhang*
Institute of Advanced Manufacturing
Technology
Ningbo Institute of Materials Technology and
Engineering, Chinese Academy of Sciences
Ningbo, China
zhangjie@nimte.ac.cn

Hai Qiao
Institute of Advanced Manufacturing
Technology
Ningbo Institute of Materials Technology and
Engineering, Chinese Academy of Sciences
Ningbo, China
qiaohai@nimte.ac.cn

Shichang Li
Semiconductor Global Solutions
Ningbo, China
ShiChang_Li@sgssemi.com

Haiyan Lan
Semiconductor Global Solutions
Ningbo, China
Echo_Lan@sgssemi.com

Zhibin Xu
Semiconductor Global Solutions
Ningbo, China
Max_Xu@sgssemi.com

Abstract—Permanent magnet linear synchronous motors (PMLSM) are widely implemented in precision manufacturing equipment with the advantages of high efficiency and high positioning accuracy. However, the thrust density of the coreless-type PMLSM is small. Due to the existence of processing errors, there is a certain gap between the actual production of the motor and the theoretical design of the motor performance, especially the winding error on the thrust ripple. Aiming at the above problems, this paper proposes a structure of a new PCB coreless-type PMLSM. This structure ensures high accuracy in coil positioning and greatly reduces costs in the manufacture of motors' actuators. In addition, this motor structure is capable of large electromagnetic thrust within the size constraints of high precision equipment. To this end, this paper presents a three-dimensional structure and analytical model of a new PCB coreless-type PMLSM. Optimization of structural parameters based on response surface method to improve motor performance. The effectiveness of the method is demonstrated by comparing the performance of the motor before and after optimization.

Keywords—Coreless-type PMLSM, Structure, Optimization, High performance.

I. INTRODUCTION

Coreless-type permanent magnet linear synchronous motors are widely used in contemporary precision machining platforms due to their low thrust ripple, high positioning accuracy, and fast dynamic response characteristics[1-3]. At the same time, conventional coreless-type PMLSMs have disadvantages such as small output thrust and low thrust bulk density. Without the fixed role of the core, the winding is prone to large errors in winding, affecting the actual performance of the motor.

Therefore, in order to improve the output thrust and electromagnetic performance of coreless-type PMLSMs, many new topologies have been proposed to optimize the motor performance in recent years. S. Qiu et al. reduced the side-end reluctance and optimized the flux density by adding a

magnetically conductive block to the side-end of the motor[4]. Z. Xie et al. improved the motor thrust density and suppressed the thrust ripple through the Halbach structure and double-layer asymmetric winding structure, but the structure is more complicated, and the winding is more difficult and not easy to glue[5]. Z. Jiao et al. proposed a new composite Halbach array structure, which can effectively improve the output performance of the motor, but the amount of permanent magnets is large and the processing and assembly are difficult[6]. S. G. Min et al. used the differential evolution method for structure optimization and finally obtained a set of structural parameters with better electromagnetic performance, but with low accuracy and cumbersome calculation process[7]. Based on the above research, this paper proposes a new coreless-type PMLSM topology. The structure has large thrust density and small thrust ripple to meet the needs of high precision equipment such as wafer inspection equipment. At the same time, taking into account the actual production of ironless core linear electric motor there is a certain processing error, greatly affecting the output performance of the motor, it is used in the form of PCB motor. In the manufacture of electric motorized sub-coils, PCBs can greatly reduce costs, ensure high accuracy in coil positioning, and enable coil shapes to be changed in this way. Printed windings print the windings directly onto the printed circuit board, avoiding the need for machine winding, lead wires, coil casting, epoxy curing and other steps. As a result, PCB technology can significantly reduce the thickness of parts, resulting in more compact structures and designs, as well as increased precision and reliability in the manufacturing process.

In this paper, a novel structure of coreless-type PMLSM is proposed and its parameters are optimized, and the comparison of results shows that the method has good results. A brief description of the motor's actuator and stator structure is given in Section 2. Section 3 describes the analytical model and electromagnetic characteristics of the motor. Section 4 optimizes the structural parameters of the motor. The final section provides a summary.

This work was supported by Science and Technology Innovation 2025 Major Special Program of Ningbo under grant No. 2022Z069.

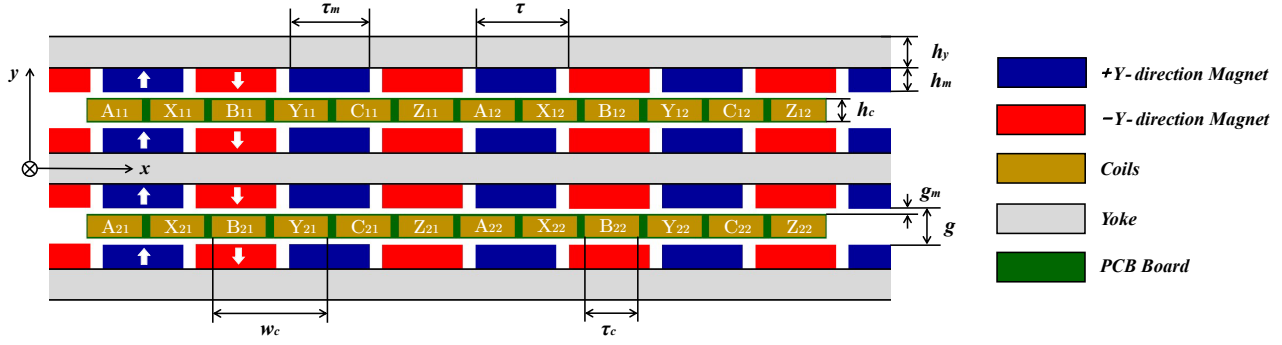


Fig. 1. Two-dimensional topology.

II. STRUCTURE AND PROPERTIES

A. Entire Structure

The novel structure proposed in this paper is an 8-pole, 6-slot coreless-type PMLSM, and Figure 1 shows the two-dimensional structure with a description of the parameters. The motor is of moving coil construction and consists of a double-layer primary and a double-layer secondary. The primary part is in the form of a printed circuit board and the winding is in the form of a non-overlapping fractional slot centralized winding. The secondary section consists of N and S staggered permanent magnets and iron yokes. The yoke has three layers, two for the back yoke and one for the center yoke. The permanent magnet has four layers, forming a double "U" structure, as shown in Figure 2. The structural parameters are demonstrated in TABLE I.

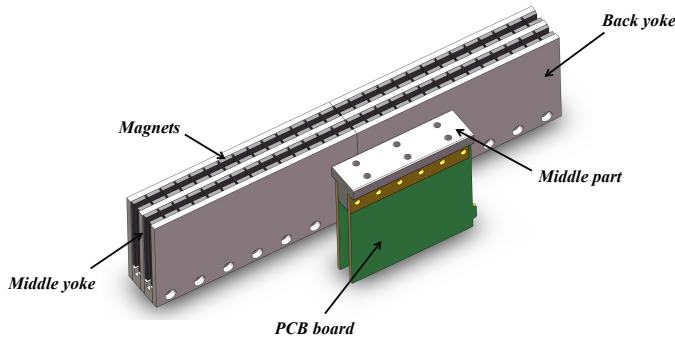


Fig. 2. Three-dimensional topology.

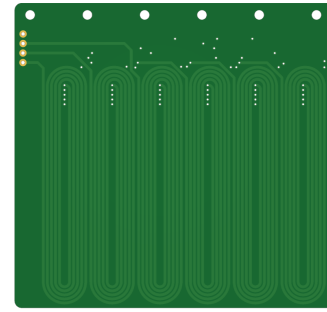
TABLE I. THE PARAMETERS OF IL-PMLM

Parameter	Symbol	Value
Yoke thickness (mm)	h_y	5
Magnet width (mm)	τ_m	13
Magnet height (mm)	h_m	4
Single side winding width (mm)	τ_c	9
Coil height (mm)	h_c	3.7
Air gap length (mm)	g_m	1

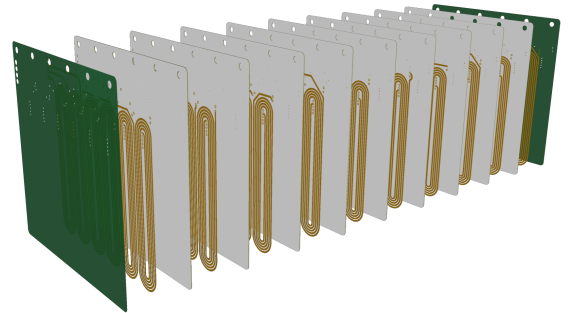
Parameter	Symbol	Value
Magnet pole pitch (mm)	τ	15
Winding width (mm)	w_c	19
Remanent magnetization (T)	B_r	1.39

B. Primary PCB Structure

Figure 3 shows a front view of a PCB board (a) with the windings unfolded (b). The layers of copper wires are connected to each other in series, and two adjacent layers are connected through holes. Unlike conventional copper wires, the windings of PCB motors are thin metal traces that are printed directly on the PCB board. Compared to circular wires, PCB winding technology is of reliable quality and precision, offers greater design flexibility, can be designed into any shape, and has greater heat dissipation capabilities.



(a)



(b)

Fig. 3. PCB Primary Structure. (a) Front view structural diagram. (b) Layered structure diagram.

The key factor in PCB coreless-type PMLSMs is the design of the windings. When designing PCB windings, the limited area of the board is utilized as much as possible. The winding form of the motor directly affects the utilization rate of the motorized motor, thus affecting the motor performance. As shown in Fig. 3, the cross sectional shape of the conductor is rectangular, flat conductor has higher fill factor and it reduces the increase in copper losses to some extent due to the reduction of end windings.

III. MAGNETIC FIELD ANALYSIS MODEL

Since the actual air gap of the coreless permanent magnet synchronous linear motor is large and the armature reaction is extremely small, this paper only analyzes the magnetic field generated by the excitation of the permanent magnets. The new structure introduced in this paper has the characteristics of symmetry along the x-direction, so only one layer of the structure is analyzed, and the layer analysis model is shown in Fig. 4.

A. Analytical Model

The following assumptions are generally made: (1) There is no change in the magnetic field along the z-axis; (2) The permeability of the secondary yoke of the linear motor is infinite; (3) The relative restitution permeability is 1.

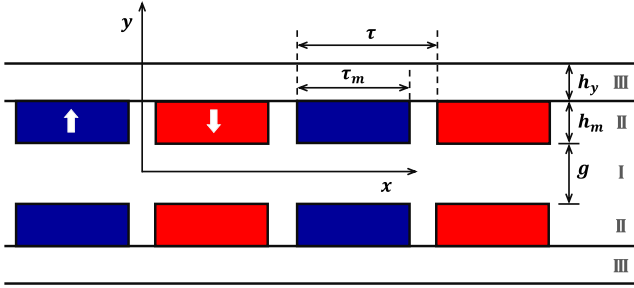


Fig. 4. Layer analysis model.

Analysis of the excitation of permanent magnets using the equivalent magnetization strength method. The equivalent magnetization strength function of a permanent magnet is expressed in Fourier series as:

$$M(x) = \sum_{k=1}^{\infty} M_k \sin \left[\frac{(2k-1)\pi}{\tau} x \right] \quad (1)$$

$$M_k = (-1)^{k+1} \frac{4}{(2k-1)\pi} M_0 \sin \left[\frac{(2k-1)\pi\tau_m}{2\tau} \right] \quad (2)$$

Based on the Maxwell's system of equations, the Poisson's system of equations is established for the air gap *Region I* and the permanent magnet *Region II*, respectively:

$$\begin{cases} \frac{\partial^2 A_{zI}}{\partial x^2} + \frac{\partial^2 A_{zI}}{\partial y^2} = 0 & \text{Region I} \\ \frac{\partial^2 A_{zII}}{\partial x^2} + \frac{\partial^2 A_{zII}}{\partial y^2} = -\mu_0 \frac{\partial M(x)}{\partial x} & \text{Region II} \end{cases} \quad (3)$$

A_I , A_{II} in Eq. (3) are the vector magnetic potentials of air gap *Region I* and permanent magnet *Region II*, respectively. The

magnetic field strength H and flux density B in the air gap region and permanent magnet region satisfy the following boundary conditions:

$$\begin{cases} H_{xI}(x, y) = H_{xII}(x, y) \Big|_{y=\frac{g}{2}-h_m} \\ B_{yI}(x, y) = B_{yII}(x, y) \Big|_{y=\frac{g}{2}-h_m} \\ B_{xII}(x, y) \Big|_{y=\frac{g}{2}} = 0 \end{cases} \quad (4)$$

The generalized solution of the equation can be obtained by the method of separated variables:

$$A_{zI}(x, y) = \sum_{k=1}^{\infty} (A_{k1} \cos m_k x + B_{k1} \sin m_k x) (C_{k1} \operatorname{sh} m_k y + D_{k1} \operatorname{ch} m_k y) \quad (5)$$

$$A_{zII}(x, y) = \sum_{k=1}^{\infty} [(A_{k2} \cos m_k x + B_{k2} \sin m_k x) (C_{k2} \operatorname{sh} m_k y + D_{k2} \operatorname{ch} m_k y) + \frac{\mu_0 M_k}{m_k} \cos m_k x] \quad (6)$$

Based on the symmetry of the vector magnetic potential with respect to the motor the equation generalization can be simplified as:

$$A_{zI}(x, y) = \sum_{k=1}^{\infty} \cos m_k x \cdot D_{k3} \operatorname{ch} m_k y \quad (7)$$

The boundary condition (4) is brought into (6) and (7) to find the coefficient equations, which leads to the vector magnetic potential expression:

$$A_{zI}(x, y) = \sum_{k=1}^{\infty} \frac{\mu_0 M_k}{m_k} \frac{\operatorname{sh}(m_k h_m)}{\operatorname{sh}(m_k \frac{g}{2})} \operatorname{ch}(m_k y) \cos(m_k x) \quad (8)$$

$$A_{zII}(x, y) = \sum_{k=1}^{\infty} \frac{\mu_0 M_k}{m_k} \left\{ -\operatorname{sh} \left[m_k \left(h_m - \frac{g}{2} \right) \right] \operatorname{sh}(m_k y) + \operatorname{sh} \left[m_k \left(h_m - \frac{g}{2} \right) \right] \frac{\operatorname{ch} \left(m_k \frac{g}{2} \right)}{\operatorname{sh} \left(m_k \frac{g}{2} \right)} \operatorname{ch}(m_k y) + 1 \right\} \cos(m_k x) \quad (9)$$

$$m_k = \frac{(2k-1)\pi}{\tau} \quad (10)$$

The expression for the magnetic flux density in each region can be obtained by taking the vector magnetic potential in the above equation and solving for the deflection:

$$B_{yI}(x, y) = \sum_{k=1}^{\infty} \frac{\mu_0 M_k \operatorname{sh}(m_k h_m)}{\operatorname{sh} \left(m_k \frac{g}{2} \right)} \operatorname{ch}(m_k y) \sin(m_k x) \quad (11)$$

$$\begin{aligned}
B_{yII}(x, y) = & \sum_{k=1}^{\infty} \mu_0 M_k \left\{ -sh \left[m_k \left(h_m - \frac{g}{2} \right) \right] sh(m_k y) \right. \\
& + sh \left[m_k \left(h_m - \frac{g}{2} \right) \right] \frac{ch \left(m_k \frac{g}{2} \right)}{sh \left(m_k \frac{g}{2} \right)} ch(m_k y) \\
& \left. + 1 \right\} \sin(m_k x) \quad (12)
\end{aligned}$$

B. Finite Element Method Comparison

Fig. 5 compares the air gap magnetometers obtained by the analytical method and the finite element simulation method for the physical air gap centerline and the mechanical air gap centerline, and the analytical values are slightly smaller than the finite element simulation values. Through comparative analysis, the equivalent magnetization strength method can be applied to the new coreless-type PMLSM of this structure.

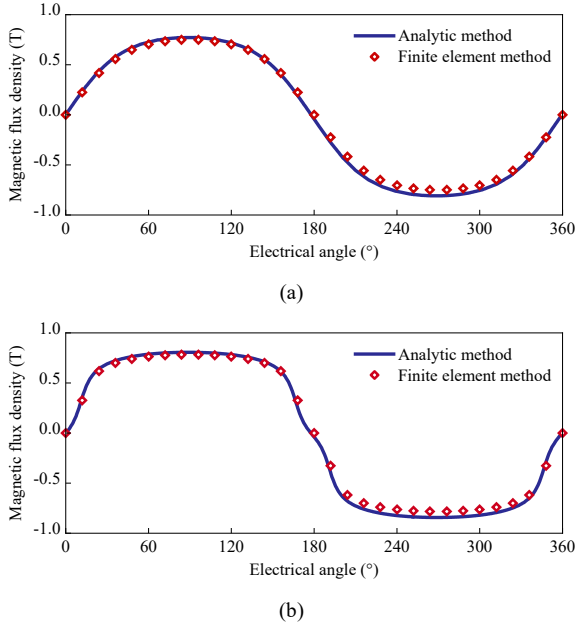


Fig. 5. Comparison of air gap magnetic density at two positions. (a) Physical air gap centerline. (b) Mechanical Air Gap Centerline.

IV. PARAMETER OPTIMIZATION

Response surface method is a statistical and optimization method to solve multivariate problems by using reasonable experimental design methods and obtaining certain data through experiments, adopting multivariate quadratic regression equations to fit the functional relationship between the factors and the response values, and seeking the optimal structural parameters through the analysis of regression equations.

The permanent magnet height (h_m), permanent magnet width (τ_m) and single side winding width (τ_c) are determined as the optimized parameters for motor output performance by Taguchi method. In this paper, Box-Behnken response surface model is constructed by finite element simulation, orthogonal experimental matrix is established for the three sensitive parameters, and the thrust performance under each combination

is derived through finite element analysis, and the response surface orthogonal test table is shown in TABLE II.

TABLE II. RESPONSE SURFACE ORTHOGONAL TEST TABLE

No.	h_m	τ_m	τ_c	Force	Ripple
1	4.5	13	9	206.63	0.890
2	4	12.5	8	216.07	0.356
3	4.5	12.5	8.5	214.15	0.359
4	4	12.5	9	198.93	0.401
5	4.5	12.5	8.5	214.15	0.359
6	4.5	12	9	201.27	0.277
7	5	12	8.5	215.25	0.165
8	5	13	8.5	221.7	0.698
9	4.5	13	8	225.94	0.477
10	4.5	12	8	219.4	0.164
11	5	12.5	8	227.9	0.348
12	4	13	8.5	210.82	0.720
13	4	12	8.5	204.74	0.147
14	4.5	12.5	8.5	214.15	0.359
15	5	12.5	9	209.06	0.393

Based on the least squares estimation, the response surface mathematical model equations for the output thrust and thrust ripple of the coreless-type PMLSM are collated and obtained, respectively:

$$\begin{aligned}
F = & -339.68375 + 44.8275 * h_m + 49.5975 * \tau_m + \\
& 37.28 * \tau_c + 0.37 * h_m * \tau_m - 1.7 * h_m * \tau_c - 1.18 * \tau_m * \\
& \tau_c - 2.685 * h_m^2 - 1.405 * \tau_m^2 - 1.955 * \tau_c^2 \quad (13)
\end{aligned}$$

$$\begin{aligned}
F_r = & 74.34653 + 0.561122 * h_m - 9.40093 * \tau_m - \\
& 4.77924 * \tau_c - 0.040155 * h_m * \tau_m + 0.00139 * h_m * \tau_c + \\
& 0.299267 * \tau_m * \tau_c - 0.008437 * h_m^2 + 0.301826 * \tau_m^2 + \\
& 0.069779 * \tau_c^2 \quad (14)
\end{aligned}$$

Fig. 6 depicts the effect of the interaction between the factors of the response surface model of the coreless-type PMLSM output thrust and thrust ripple for the novel structure, from which the magnitude of the response surface variation of each parameter can be visualized. As can be seen in Fig. 6, the interaction effects of both permanent magnet height and winding width on the output thrust are more significant at the coreless-type PMLSM mechanical air gap length of 1 mm. Compared with the permanent magnet width, the response surface changes more with the increase of the permanent magnet height, indicating that the permanent magnet height has a stronger effect on the response surface than the permanent magnet width. The response surface images of the thrust ripple show that the change in the width of the permanent magnet has the strongest effect on the magnitude of the response surface change.

The optimized motor structure parameters are shown in TABLE III.

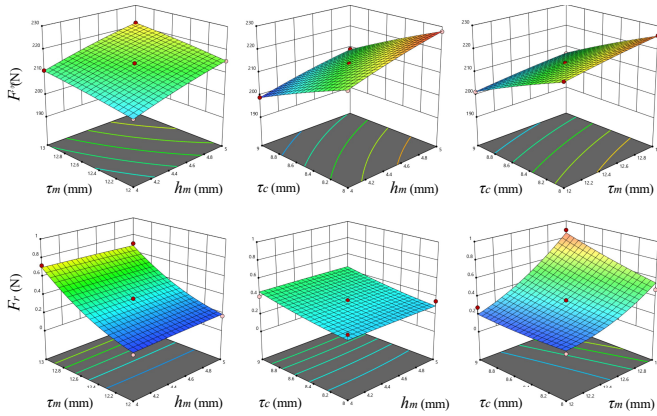


Fig. 6. Response surface.

TABLE III. COMPARISON OF ORIGINAL AND OPTIMIZED PARAMETERS

Parameter	Original	Optimal
h_m (mm)	4	5
τ_m (mm)	13	12.3
τ_c (mm)	9	8
F (N)	192.74	226.50
F_r (%)	0.75%	0.27%

The finite element method is used to compare the two sets of parameters before and after optimization at the applied current of 4A. The output thrust of the optimal motor is 226.50N, which is increased by 17.5% compared to the pre-optimization. The thrust ripple is 0.27% and the comparison shows that the thrust performance of the motor is greatly improved. Thrust image comparisons are shown in Fig. 7.

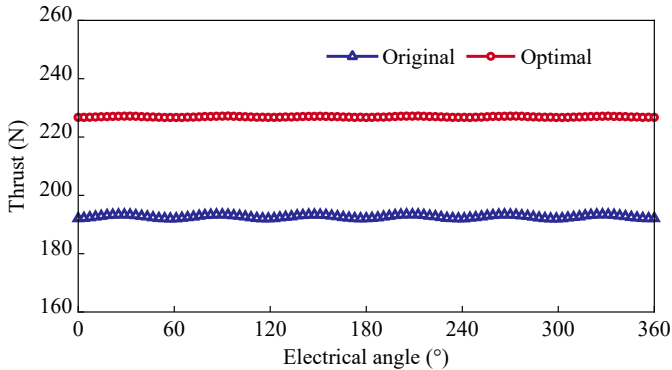


Fig. 7. Thrust comparison.

V. CONCLUSION

In this paper, the topology of a new coreless-type PMLSM is presented, where the motor's actuator is assembled using a PCB board and the actuator has a double "U" structure. The excitation magnetic field of the motor is calculated using the equivalent magnetization strength method, and the feasibility of

the method is verified by comparison with finite element simulation. Based on the response surface methodology, the sensitive parameters are optimized and analyzed, and finally the structural parameters with higher performance and lower cost are obtained.

The final obtained coreless-type PMLSM has an output thrust of 226.50N and a thrust ripple of 0.27%, which meets the application requirements of high-precision equipment.

REFERENCES

- [1] J. M. M. Rovers, J. W. Jansen and E. A. Lomonova, "Analytical Calculation of the Force Between a Rectangular Coil and a Cuboidal Permanent Magnet," in *IEEE Transactions on Magnetics*, vol. 46, no. 6, pp. 1656-1659, June 2010.
- [2] L. Li, J. Zhang, S. Qiu, H. Huang, W. Yan and C. Zhang, "Analysis of Structural Tolerance Influences on Thrust Ripple of U-Shaped Ironless Permanent Magnet Linear Motor," *IECON 2023- 49th Annual Conference of the IEEE Industrial Electronics Society*, Singapore, Singapore, 2023, pp. 1-6.
- [3] Z. Pei, J. Zhao, J. Song, K. Zong, Z. He and Y. Zhou, "Temperature Field Calculation and Water-Cooling Structure Design of Coreless Permanent Magnet Synchronous Linear Motor," in *IEEE Transactions on Industrial Electronics*, vol. 68, no. 2, pp. 1065-1076, Feb. 2021.
- [4] S. Qiu, J. Zhang, X. Sun, C. Zhang, Y. Gao and R. Li, "Magnetic Field Optimization of U-type Ironless Permanent Magnet Linear Motor Using Magnetic Permeable Block," *2021 13th International Symposium on Linear Drives for Industry Applications (LDIA)*, Wuhan, China, 2021, pp. 1-4.
- [5] Z. Xie, Q. Lu, W. Mei and Y. Li, "Improved Analytical Modeling of a Novel Ironless Linear Synchronous Machine With Asymmetrical Double-Layer Winding Topology," in *IEEE Transactions on Industry Applications*, vol. 57, no. 2, pp. 1411-1419, March-April 2021..
- [6] Z. Jiao, T. Wang and L. Yan, "Design of a Tubular Linear Oscillating Motor With a Novel Compound Halbach Magnet Array," in *IEEE/ASME Transactions on Mechatronics*, vol. 22, no. 1, pp. 498-508, Feb. 2017.
- [7] S. G. Min and B. Sarlioglu, "3-D Performance Analysis and Multiobjective Optimization of Coreless-Type PM Linear Synchronous Motors," in *IEEE Transactions on Industrial Electronics*, vol. 65, no. 2, pp. 1855-1864, Feb. 2018.